Domain wall dynamics in an optical Kerr cavity

Víctor J. Sánchez-Morcillo, Víctor Espinosa, and Isabel Pérez-Arjona
Departament de Física Aplicada, Escuela Politècnica Superior de Gandia, Universitat Politècnica de Valencia, Ctra. Natzaret-Oliva s/n, 46730 Grau de Gandia, Spain

Fernando Silva, Germán J. de Valcárcel, and Eugenio Roldán
Departament d'Òptica, Universitat de València, Dr. Moliner 50, 46100-Burjassot, Spain
(Received 28 October 2004; revised manuscript received 7 March 2005; published 22 June 2005)

An anisotropic (dichroic) optical cavity containing a self-focusing Kerr medium is shown to display a bifurcation between static—Ising—and moving—Bloch—domain walls, the so-called nonequilibrium Ising-Bloch transition (NIB). Bloch walls can show regular or irregular temporal behavior, in particular, bursting and spiking. These phenomena are interpreted in terms of the spatiotemporal dynamics of the extended patterns connected by the wall, which display complex dynamical behavior as well. Domain wall interaction, including the formation of bound states is also addressed.

DOI: 10.1103/PhysRevE.71.066209 PACS number(s): 47.54.+r, 42.65.Sf, 42.50.Md

I. INTRODUCTION

Domain walls are localized structures typical of spatially extended systems with broken phase invariance, where two or more homogeneous states with different phases occupy different patches, the walls being defects connecting two of such states or domains. Two different types of walls can exist in systems described by a complex order parameter, namely Ising and Bloch walls, which differ in the way the phase changes between the two domains as the wall is crossed: An Ising wall is characterized by a discontinuous variation of the field phase across the wall, whereas in a Bloch wall the phase angle rotates continuously accross the wall. As this rotation can occur in two different senses Bloch walls are chiral. (Contrarily, the Ising wall is not chiral.) Alternatively, the order parameter is null at the core of an Ising wall, while in a Bloch wall the order parameter does not vanish at any point. For this reason, Ising and Bloch walls are often referred to as dark and grey solitons, respectively. When the system dynamics do not derive from a potential, other crucial differences between Ising and Bloch walls refer to their dynamics: Ising walls are stationary (static), while Bloch walls move with a velocity related to their chirality.

Both types of domain walls may exist in different parameter regions, and in this case they bifurcate one into another via a nonequilibrium Ising-Bloch (IB) transition [1,2], which can be interpreted as a bifurcation of the wall chirality [1]. The IB transition has been found in systems of very different nature, such as nematic liquid crystals [3] or reaction-diffusion systems [4]. In the optical context, the phenomenon has been predicted to occur in type I [5] and type II [6] optical parametric oscillators; from the experimental point of view it is to be mentioned a related study [7] where Larionova *et al.* have analyzed the dynamics of two-dimensional phase domains in a photorefractive oscillator in a degenerate four-wave mixing configuration. Within the same (closed) wall they found both Bloch-type and Ising-type segments. They did not observe, however, the nonequilibrium IB transition, probably because of the two-dimensional (2D) character of their system, which complicates the dynamics of domain walls with curvature effects. In fact the first experimental observation of the nonequilibrium IB transition in optics has been confirmed very recently in the (transversely) one-dimensional version of the same device [8]. The possibility of domain walls as stable states has a particular interest in nonlinear optical systems, given the potential use of localized structures in all-optical signal processing. In nonlinear optical cavities, the structures develop in the transverse plane, perpendicular to the resonator axis, and can be controlled by external parameters [9].

Optical systems with a Kerr nonlinearity have been shown to exhibit a rich spatiotemporal dynamics, see Ref. [10] and references therein for details. Concerning the nonequilibrium Ising-Bloch transition, the Kerr cavity, consisting of an optical resonator filled with a Kerr medium and driven by a external coherent field, is a good candidate for exhibiting it, as this system presents the basic requirement of broken phase invariance. The original model proposed by Lugiato and Lefever [11] was later extended in Ref. [12] to include the vector character of the light fields, what allows to describe instabilities of the light polarization state. This work was extended in Ref. [13] where the case of elliptically polarized input was considered and in Ref. [14] where two-dimensional domain walls in the form of dark-ring solitons were studied.

Recently these works were generalized by considering the possibility of dichroism and/or birefringence in the optical cavity for the two linear polarization components [15–17]. It was shown that large enough cavity anisotropy or birefringence substantially modifies the dynamics of the system. In particular, they allow for the polarization instability to rule pattern formation in self-focusing Kerr cavities, something that does not occur in isotropic cavities (without birefringence or dichroism) [12]. Moreover, as the polarization instability can be subcritical for large enough dichroism or birefringence [16,17] bright cavity solitons can exist, which in this case are polarization solitons [16,17]. In Ref. [16] it was also shown that in the limit of large anisotropy (when the losses of the two polarization components are very different in magnitude), the dynamics of the system can be

described by a single order parameter obeying a universal equation, namely the parametrically driven, damped nonlinear Schrödinger equation (PDNLSE). For our purposes the recent prediction [18] that the PDNLSE contains an IB transition and that Ising and Bloch domain walls can connect either spatially uniform or patterned states is of special relevance. This equation has been derived in different contexts (see Ref. [18]). In particular, in the optical context, the PDNLSE has been shown to describe (apart from the anisotropic Kerr resonator [16]) the degenerate optical parametric oscillator [19,20] and optical fiber loops with parametric amplification [21].

However, despite the generality of the results obtained in Ref. [18], their applicability to the Kerr cavity is strictly valid only in the case of strong anisotropy, a very restrictive condition. In this paper we consider the more realistic case of a Kerr cavity with moderate anisotropy as discussed in Sec. II, where the symmetries of the model and the feasibility of domain walls are discussed. The pattern forming properties of this system are investigated in Sec. III. Ising and Bloch walls are then shown to be solutions of the system and the IB transition between them is characterized in Sec. IV. For small detunings, the usual scenario of IB transition and Bloch wall dynamics is found. For larger detunings, the dynamics of domain walls shows features typical of excitable systems, such as spiking and bursting during the domain wall evolution, as discussed in Sec. VI. The collisions between walls and the formation of bound states is preliminarily considered in Sec. V. Finally the main conclusions of the work are highlighted in Sec. VII.

II. MODEL AND HOMOGENEOUS SOLUTIONS

The system considered in this paper is an optical resonator with plane mirrors filled with an isotropic $\chi^{(3)}$ medium of self-focusing type and driven by a spatially homogeneous linearly polarized coherent field of amplitude E (taken real without loss of generality) that propagates along the resonator axis z. The resonator is anisotropic (dichroic), i.e., the two intracavity field polarization components A_0 and A_1 (parallel and orthogonal to the input field, respectively) experience different linear losses (with associated cavity linewidths γ_0 and γ_1, respectively). In order to avoid curvature effects that strongly influence domain wall dynamics, we assume a transversely one-dimensional (1D) problem (that can be experimentally achieved with a slab waveguide geometry that confines the fields along one transverse dimension (say y), or with rectangular slits placed in appropriate planes [22]). The adimensional model equations for such a system in the mean field limit read [16,17]

$$\partial_t A_0 = -(\gamma + i\Delta_0)A_0 + i\left(|A_0|^2 A_0 + \mathcal{A}|A_1|^2 A_0 + \frac{\mathcal{B}}{2}A_1^2 A_0^*\right) + i\partial_x^2 A_0 + \gamma E, \tag{1}$$

$$\partial_t A_1 = -(1 + i\Delta_1)A_1 + i\left(|A_1|^2 A_1 + \mathcal{A}|A_0|^2 A_1 + \frac{\mathcal{B}}{2}A_0^2 A_1^*\right) + i\partial_x^2 A_1, \tag{2}$$

where $\Delta_0 = (\omega_0 - \omega)/\gamma_1$ and $\Delta_1 = (\omega_1 - \omega)/\gamma_1$ are normalized cavity detunings (ω is the angular frequency of the input field and $\omega_{0,1}$ are the frequencies of the cavity longitudinal modes with polarization parallel and orthogonal to the input closest to ω), $\gamma = \gamma_0/\gamma_1$ is the cavity anisotropy parameter; ∂_x^2 accounts for diffraction (the transverse spatial coordinate x is normalized to the diffraction coefficient) and t is time normalized to γ_1^{-1}. Finally, $\mathcal{A}$ and $\mathcal{B}$ are the Maker and Terhune coefficients, which verify $\mathcal{A} + (\mathcal{B}/2) = 1$ for isotropic media [23], which we consider. For details on the normalizations see Ref. [15].

In Refs. [12–14], the pattern formation properties of this model have been studied for $\gamma = 1$ and $\Delta_1 = \Delta_0$. We extended the model to the anisotropic cavity ($\gamma \neq 1$) first considering the plane-wave model (no diffraction) [15] and then considering pattern formation [16], where we concentrated in the limit of large cavity anisotropy and demonstrated that the PDNLSE describes the system in this limit. Later, in Ref. [17] we studied pattern formation and localized structures due to birefringence ($\Delta_0 \neq \Delta_1$).

In the following, the case $\Delta_0 = \Delta_1 \equiv \Delta$ (no birefringence) is considered. Also we restrict the study to the case when the nonlinear material is a liquid (e.g., CS_2), for which $\mathcal{A} = 1/4$ and $\mathcal{B} = 3/2$ [23]. This makes that our results could apply, e.g., to cells of liquid crystal in the isotropic phase (nematic liquid crystals, which have a much larger nonlinearity, are not covered by our analysis as they are *anisotropic* nonlinear media).

Most relevant for our study are the symmetries supported by Eqs. (1) and (2). In particular the term γE in Eq. (1) completely breaks the phase symmetry of field A_0. Nevertheless, the model still supports the discrete symmetry $(A_0, A_1) \rightarrow (A_0, -A_1)$. [Note that the four-wave mixing term—the one multiplied by $\mathcal{B}/2$ in Eq. (2)—breaks the continuous phase symmetry.] This symmetry means that whenever a state $(A_0(x,t), A_1(x,t))$ is a solution of the system, another solution $(A_0(x,t), -A_1(x,t))$ exists as well that is dynamically equivalent (has the same dynamical properties like stability, etc.) to the former. As A_0 and A_1 correspond to the two orthogonal components of the light electric field vector, the above symmetry relates two equivalent solutions having opposite helicity, apart from a different polarization ellipse orientation. This symmetry thus opens the possibility of exciting domain walls that join asymptotically two of such symmetric states. On the other hand, the reflection ($x \rightarrow -x$) and translation ($x \rightarrow x + x_0$) invariances of the problem imply that if a Bloch wall of given chirality exists, another, equivalent one of opposite chirality also exists, and both move in opposite directions [1,8,18].

The existence conditions and dynamic behavior of domain walls, the main subject of this paper, is strongly related with the stability properties of the homogeneous solutions connected by the walls. In the system described by Eqs. (1) and (2), these solutions have been analyzed in Refs. [15,17], and we review here the main results.

According to the polarization state of the intracavity field two kinds of steady homogeneous solutions are possible, (i) the *linearly polarized state*, with intensities $I_1 \equiv |A_1^2| = 0$ and $I_0 \equiv |A_0^2|$ given by the solutions of

$$\gamma^2 E^2 = [\gamma^2 + (\Delta - I_0)^2]I_0, \tag{3}$$

and (ii) the *elliptically polarized state*, with intensities determined by

$$\gamma^2 E^2 I_0 = (I_1 + \gamma I_0)^2 + [(\Delta - I_1)I_1 - (\Delta - I_0)I_0]^2, \qquad (4)$$

$$I_1 = \Delta - \mathcal{A} I_0 \pm \sqrt{\left(\frac{\mathcal{B}}{2} I_0\right)^2 - 1}. \qquad (5)$$

The linearly polarized solution Eq. (3) shows a multivalued character when $\Delta > \sqrt{3}\gamma$ [15]. The elliptically polarized solution Eq. (4) was analyzed in detail in Ref. [15] and can be a multivalued function as well.

The cavity anisotropy parameter γ plays an important role on the character of the polarization instability (i.e., the bifurcation affecting the linearly polarized solution that sets the onset of eliptically polarized emission), as shown in Refs. [15,17]. In particular the polarization instability can become subcritical for $\gamma > 2$ (the exact value at which this occurs depends on the detuning value) whenever $\Delta > 1/3$. In this case bright cavity solitons can be supported by the system at low pumpings [16]. More important for the present study is the fact that for large γ the anisotropic Kerr cavity model can be reduced to a PDNLSE, which exhibits an IB transition [18]. This implies that the anisotropic Kerr cavity will exhibit the same phenomenon for large enough γ. In order to test the universality of this phenomenon we investigate here a cavity with moderate anisotropy and take $\gamma = 3.5$ for definiteness. We note that for this value of γ the model cannot be rigorously reduced to a PDNLSE and then some extra features can be expected.

III. THE PATTERN FORMING INSTABILITIES

The stability of the linearly polarized solution (3) against space-dependent perturbations was analyzed in Refs. [16,17], where analytical expressions for the different boundaries and wave number of the emerging patterns were obtained. In Fig. 1 the stability of the different solutions is shown on the plane E-Δ, which are the only free parameters. In the figure, the linearly polarized solution (3) is stable below curve E_1, which corresponds to the polarization instability. Above this curve the linearly polarized state is no more a stable solution and gives rise to the elliptically polarized solution (4) and (5). In its turn, this last solution exists above line E_2, i.e., there is a domain of coexistence between the linearly and elliptically polarized solutions, marked in the figure as BS, between lines E_1 and E_2.

We consider now the existence of pattern forming instabilities of the elliptically polarized solution (4) and (5), which are of relevance for the analysis of the dynamics of domain walls performed below. Following the usual procedure, we consider perturbations of the homogeneous solutions in the form $\delta A_i(x,t) = \delta A_i \exp(\lambda t + ikx)$, and $\mathrm{Re}(\lambda) = 0$ signals a bifurcation. Unlike the case of the linearly polarized solution [16,17], the stability analysis is now quite involved and analytic expressions cannot be obtained. Instead, we perform a numerical analysis of the eigenvalues λ to determine the instability boundaries.

The pattern formation instability boundary affecting the elliptically polarized solution (4) and (5) corresponds to the

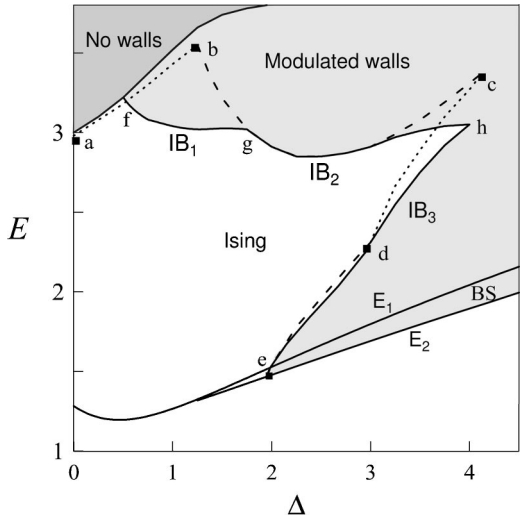

FIG. 1. Bifurcation diagram of homogeneous solutions for $\mathcal{A} = 1/4$, $\mathcal{B} = 3/2$, $\Delta_0 = \Delta_1 = \Delta$, and $\gamma = 3.5$, together with the boundaries of Ising-Bloch transitions. See text for details.

piecewise curve (with dashed and dotted segments) joining the points *a*–*e*. Beyond this line (shadowed area), the elliptically polarized solution is modulationally unstable.

The complex form of this boundary follows from the dependence of the real part of the largest eigenvalue with the wave number of the perturbation. As shown in Fig. 2, the real part of the eigenvalue (solid line) evaluated for parameters corresponding to point (b) in Fig. 1 shows two maxima at different wave numbers. Depending on the parameter setting the threshold is minimum for the smallest wave number (dashed lines *b*–*c* and *d*–*e*) or for the largest wave number (dotted lines *a*–*b* and *c*–*d*). Consequently, the points denoted by *b*, *c*, and *d* in the figure correspond to codimension-2 points, where the instability is reached at two different wave numbers simultaneously. Furthermore, the imaginary part of the eigenvalue is null in the first cases (dashed lines *b*–*c* and *d*–*e*), thus corresponding to the emergence of stationary patterns, but non-null in the second cases (dotted lines *a*–*b* and *c*–*d*), see Fig. 2, thus corresponding to a Hopf bifurcation

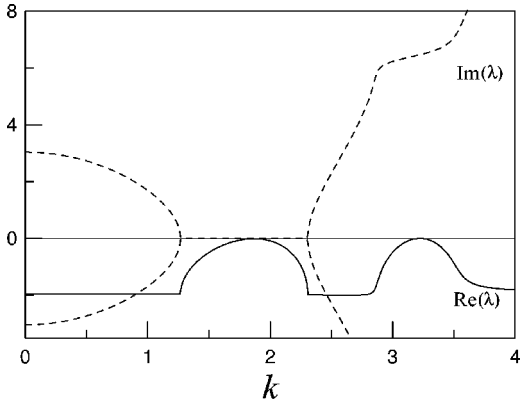

FIG. 2. Growth rate of the perturbations of the homogeneous solutions as a function of the spatial wave number, near a codimension-2 point for $\Delta = 1.25$ and $E = 3.5$. The rest of the parameters are the same as in Fig. 1.

that gives rise to the appearance of dynamic patterns whose amplitude oscillates in time. Finally, as stated, the region marked with BS in Fig. 1 denotes the domain of coexistence between linearly and elliptically polarized states. When this coexistence is bistable and one of the states (the elliptically polarized state in this case) is spatially modulated (shadowed region), bright cavity solitons can be also excited [16,17].

IV. THE ISING-BLOCH TRANSITION

We performed the numerical integration of Eqs. (1) and (2) with a split-step algorithm, for $\mathcal{A}=1/4$, $\mathcal{B}=3/2$, $\Delta_0=\Delta_1 \equiv \Delta$, and $\gamma=3.5$. Periodic boundary conditions were used that impose an even number of walls in the transverse domain. A spatial grid of 2048 points was used and the temporal step was lowered down to $\Delta t=0.001$ in order to obtain Δt-independent results. As an initial condition, two walls were placed symmetrically with respect to the center of the integration window. Several integration region lengths L were investigated. Results shown here correspond to the choice $L=20\sqrt{5}$, which ensured enough spatial separation between the two walls in order to avoid their mutual interaction during the initial stage of the evolution. For some parameter settings the walls reached a static configuration after a transient, having fixed their position across the transverse plane. In such cases it was assessed that walls were Ising ones by verifying that the complex field A_1 was zero at the wall core. For other parameter values walls reached a moving configuration and were identified as Bloch walls as there was no point in the transverse plane where the complex field A_1 was zero. Note that the following analysis of the results refers to the cross polarized component A_1 that is the one in which domain walls can be clearly identified as dark solitons [16] as walls join two domains where the values of A_1 have opposite signs (phases) as discussed.

Figure 1 summarizes our numerical findings. For low values of both pump E and detuning Δ (inside the region labeled "Ising," delimited by the solid lines joining points *a–f–g–h–d–e*, and line E_2) stable Ising walls are found. These Ising walls connect homogeneous states in most of this region, except in the thin white areas at the right of the dashed line *d–e* and the dotted line *c–d*, where they connect patterned states, in agreement with the linear stability analysis discussed above. By increasing the pump or the detuning from this region we observe IB transitions, marked with solid lines *f–g–h–d–e*, where Ising walls are replaced by Bloch walls.

Before commenting the differences between the various Ising-Bloch transition lines (IB_1, IB_2, and IB_3), let us comment about what happens in the small region above line *a–b*, where the behavior is somewhat anomalous. In the small domain between this line and the dark-grey shadowed area marked as "No walls" the walls are unstable, and the single pattern supported by the system are rolls. Then, strictly speaking, the domain "No walls" extends until the line *a–b*. If we have left this domain without including it in the "No walls" domain it is just because in it a very long transient behavior in the dynamics of the walls is observed until walls eventually disappear and the system develops a spatially periodic state. This behavior (longest transient) is in contrast with what happens in the "No walls" domain, where domain walls disappear sharply.

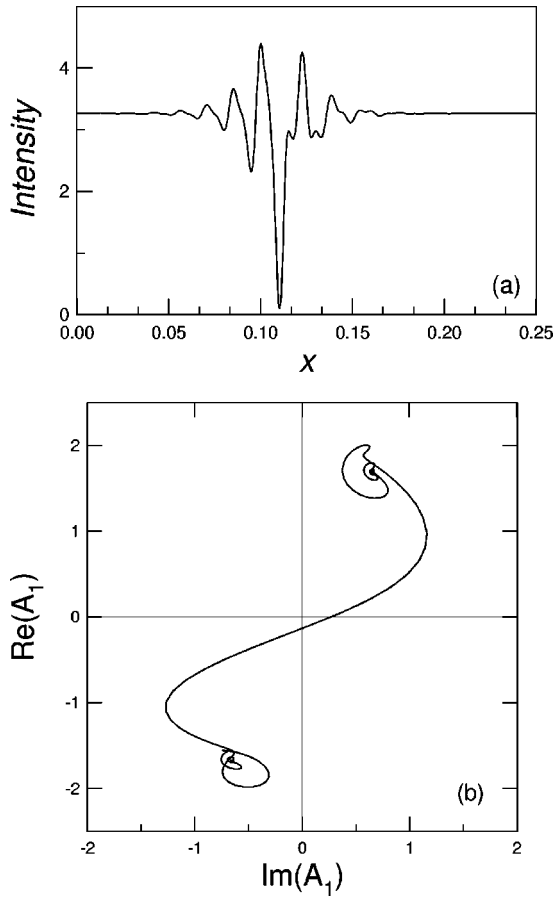

FIG. 3. Example of a pair of Bloch walls numerically obtained for the parameters $\Delta=0.8$ and $E=3.25$ (the rest of the parameters are the same as in Fig. 1). Intensity distribution (a) and parametric representation (b).

At the right of the point *f*, when increasing the pump, two different regimes can be clearly distinguished, depending on detuning. For small detunings the transition is denoted by IB_1 in Fig. 1 (continuous line), and in this case the Bloch walls (that exist inside the "triangle" *f–b–g*) connect homogeneous states. For the chosen values of the parameters, this regime exists up to $\Delta=1.75$. For larger detunings, the transition is mainly ruled by the pattern forming instability experienced by the domains joined by the walls (IB_2 in Fig. 1, represented by the continuous curve). Note that, for moderate detunings (in the center of the plot), the IB and pattern forming boundaries are nearly coincident. In this case the Bloch walls always connect patterned states. Finally, for small pump but large detunings, another region IB_3 of Bloch walls is found (right-hand side of the curve *h–d–e*). The Bloch walls in this region move with an extremely small, random velocity, similarly to what happens in the PDNLSE without diffusion or saturation terms [18].

An example of a Bloch wall corresponding to the transition IB_1, obtained for $\Delta=0.8$ and $E=3.25$, is shown in Fig. 3. In Fig. 3(a) the intensity distribution in transverse space near the core of the wall is given, and in Fig. 3(b) we show the

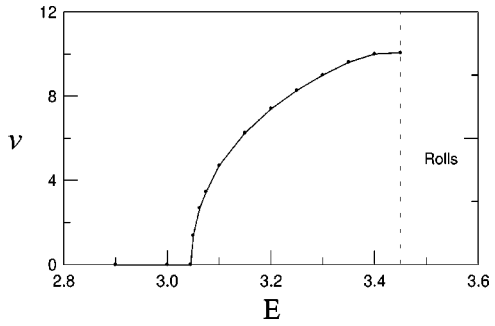

FIG. 4. Bifurcation diagram of the velocity of the walls for $\Delta = 1$ (the rest of the parameters are the same as in Fig. 1). Dashed line shows the boundary of the pattern forming instability

corresponding phase portrait (i.e., a plot of the real versus the imaginary part of the field). Both pictures are alternative representations where the Bloch character of the wall is evidenced. The intensity at the wall core is small, but non-null, Fig. 3(a), and a smooth variation of the phase between the domains separated by the wall is appreciated in the parametric plot in Fig. 3(b). For these parameters, the homogeneous solutions which constitute the domains connected by the wall are modulationally stable.

As stated in the introduction, an essential feature of Bloch walls in nonvariational systems is that, contrary to Ising walls, they move in the transverse plane, with a velocity that depends on the parameters. For a fixed value of the detuning $\Delta = 1$, the dependence of the wall velocity with the pump is shown in Fig. 4. For this particular value of the detuning, in the region where the background solutions are modulationally unstable, the walls no longer exist as commented, since spatial modulations of the background grow and fill completely the transverse space leading eventually to a roll pattern.

Let us now describe the dynamic behavior of Bloch walls.

V. BOUND STATES

As stated in the preceding section the use of periodic boundary conditions forces that the number of domain walls that can exist within the integration window be an even number, two is the minimum. On the other hand, Bloch walls move with a velocity whose sign depends on their chirality. Then two situations are possible, namely, that the two Bloch walls have either the same or different chiralities (notice that the sign of the chirality of the Bloch walls is fixed by the initial conditions). When the chiralities are the same, the two Bloch walls move along parallel paths and no interaction between them appears (at least when their movement is regular; when it is highly irregular the chirality of the walls can change independently of each other [18]). Contrarily, when the chiralities are opposite the paths followed by the two Bloch walls intersect and a collision occurs. As a result a localized structure may appear and a bound state is formed. This bound state is a cavity soliton different from a wall. Although a detailed study of these objects falls outside the scope of the present work, and without trying to be exhaustive in their characterization, we just note that two different

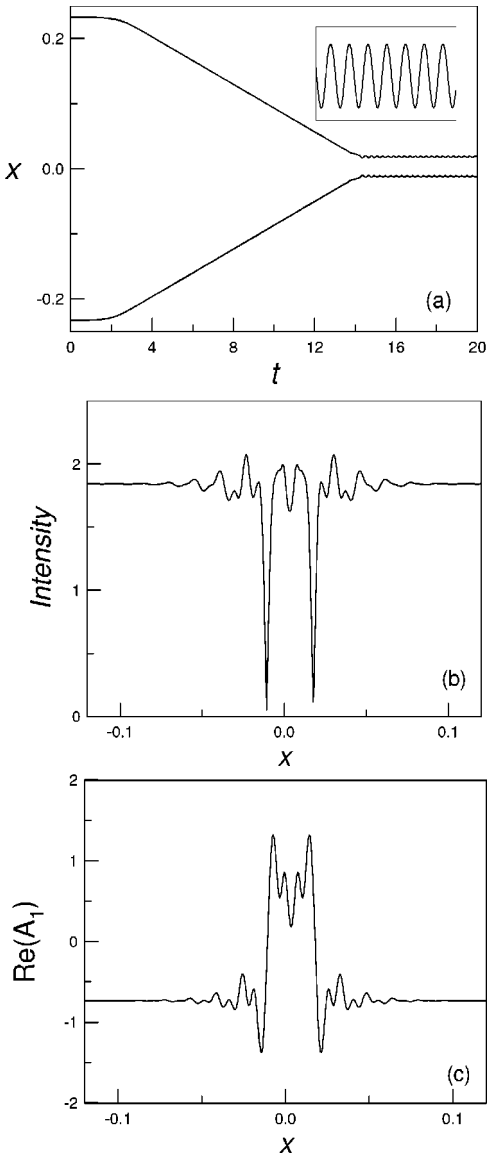

FIG. 5. Interaction of two Bloch walls with opposite chirality for $\Delta = 1$ and $E = 3.1$ (the rest of the parameters are the same as in Fig. 1). Intensity (b) and real part (c) distribution of the bound state. The inset shows the oscillatory evolution of the wall position after the interaction.

behaviors of the cavity soliton have been identified.

For small detunings (i.e., inside the triangle *f–b–g* above the region IB_1 in Fig. 1), after the collision the positions of the walls delimiting the cavity soliton perform small amplitude antiphase periodic oscillations, as shown in Fig. 5; hence the cavity soliton performs a breathing dynamics, remaining constant at its position in the transverse plane.

For higher detunings (above the region IB_2) bound states are also formed as a result of the interaction, but their dynamics is different. In these cases, after the collision, one wall is dragged by the other and the resulting bound state drifts with the velocity of one of the original Bloch walls as shown in Fig. 6.

Finally, we note that near but below the boundary *a–b*, the walls do not form bound states after the interaction, but in-

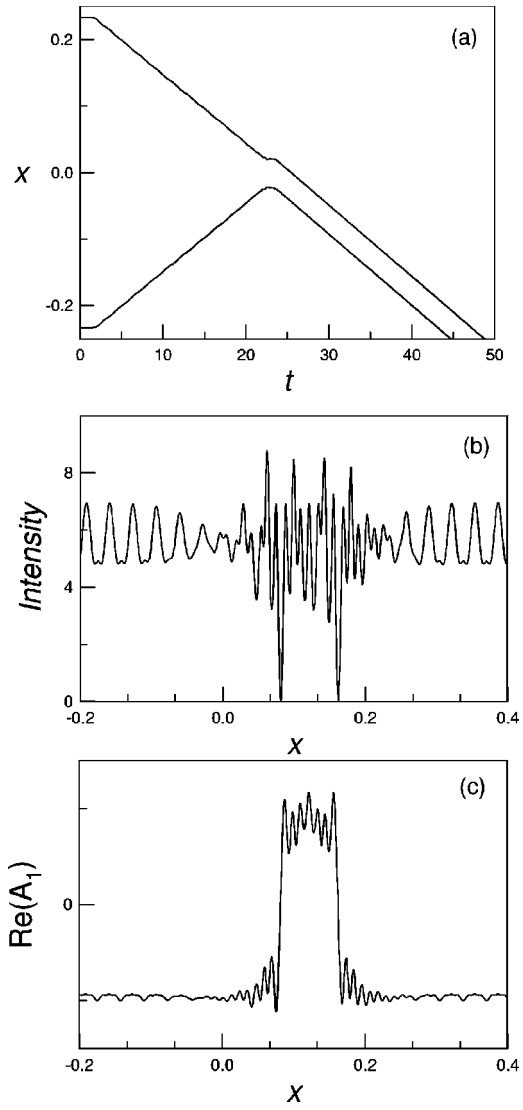

FIG. 6. Interaction of two Bloch walls with opposite chirality for $\Delta=3.25$ and $E=3$ (the rest of the parameters are the same as in Fig. 1). Intensity (b) and real part (c) distribution of the bound state.

stead bounce and exchange their chiralities. Such behavior is shown in Fig. 7.

Although it is difficult to determine the origin of these behaviors after a collision is produced, the reason for these different behaviors is very likely linked to the different dynamics of the patterned state that the walls connect, whose complicated spatiotemporal dynamics depends on the parameter set. In the next section, where we concentrate in the dynamic behavior of isolated Bloch walls, we give some clues on how the pattern dynamics affects the wall behavior.

VI. BURSTING AND SPIKING DYNAMICS OF ISOLATED DOMAIN WALLS

In the small detuning regime, Bloch walls behave in a regular manner and the motion occurs at a constant velocity as in the case shown in Fig. 4. For higher detunings however, the wall dynamics shows features which are characteristic of

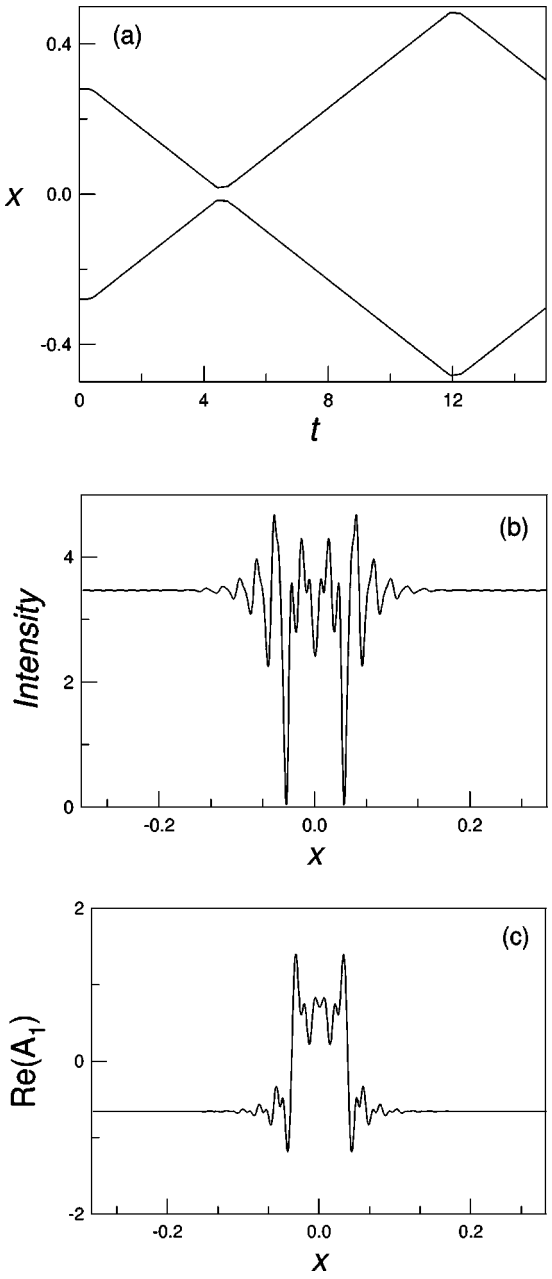

FIG. 7. Bouncing of two walls for $\Delta=0.84$ and $E=3.4$ (the rest of the parameters are the same as in Fig. 1). Intensity (b) and real part (c) distribution of the walls during the interaction.

excitable systems. The wall motion is in fact regular only close to the IB_2 transition, which nearly coincides with the pattern formation boundary, see Fig. 1. For higher pump values, wall dynamics is characterized by an irregular behavior of the wall position. We report next several numerical examples of such irregular motion, obtained for $E=3.5$ and different values of the detuning Δ.

In Fig. 8, a bursting phenomenon (the appearance of almost periodic oscillations during time intervals of arbitrary duration), is observed both in the wall position, Fig. 8(a), and chirality, Fig. 8(b), for $\Delta=2.25$. [We used the definition of chirality $\chi=\mathrm{Im}(A_1^*\partial_x A_1)|_{x=x_0}$ [18] where x_0 denotes the point where the wall intensity $|A_1|^2$ is at its minimum.] After ex-

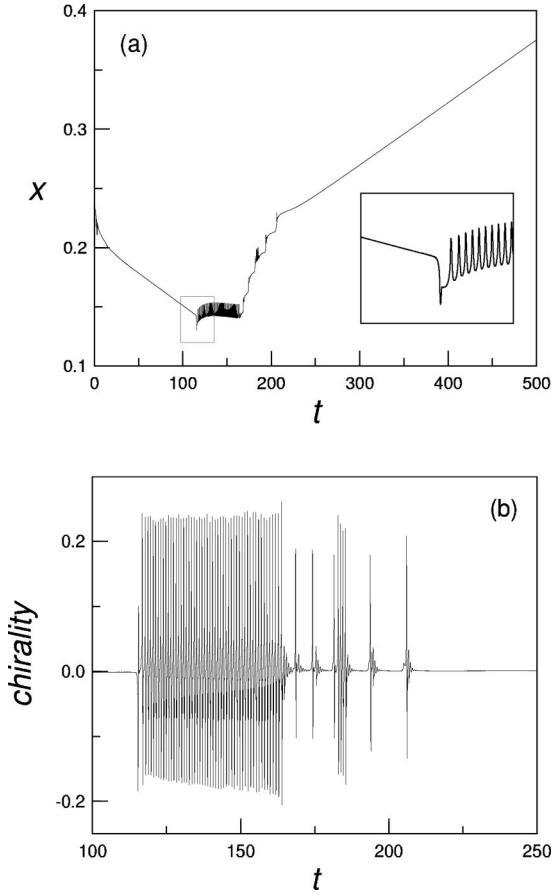

FIG. 8. Bursting of the wall position (a) and chirality (b), obtained for $\Delta=2.25$, $E=3.5$ (the rest of the parameters are the same as in Fig. 1). Inset shows the oscillations during the burst.

periencing several bursts, the wall velocity turns to be constant again, but in this case with a chirality of opposite sign with respect to the initial one. During the steady motion, the chirality takes a very small value, $\chi \approx 10^{-3}$, and consequently the change in sign is not appreciated in Fig. 8(b), owing to the scale imposed by the bursting events. However, this change is manifested in Fig. 8(a) as a change in the sign of the wall velocity. The number of bursts and final chirality depends in general on the parameter values and initial conditions, such as the amplitude and the relative distance of the two initial walls.

A slight increase in the detuning leads to a qualitatively different behavior, namely a spiking in the wall position. An example is shown in Fig. 9, obtained for $\Delta=2.5$. In this case the bursts appear periodically in time, in the form of spikes. The intensity distribution of the Bloch wall during the spiking regime is shown in Fig. 10. The wall connects two patterned states with different spatial distributions. The pattern on the right-hand side of the wall in Fig. 10 is spatially harmonic, contains a single spatial frequency, while the pattern of the left-hand side of the wall is biperiodic, and both a fundamental and a small amplitude second spatial harmonic are present. This particular structure of the domain walls has been observed in all the numerical simulations in the irregular regime, and seems to be at the root of the complex behavior exhibited by the wall dynamics.

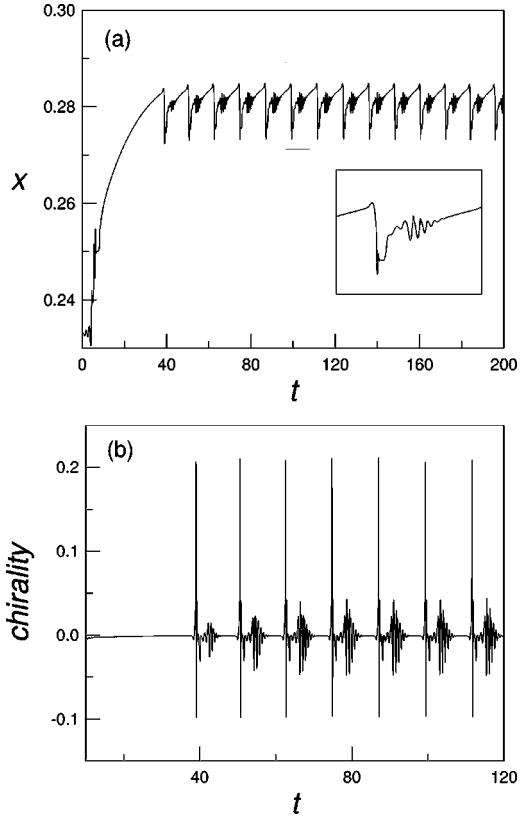

FIG. 9. Spiking behavior of the wall position (a) and chirality (b), obtained for $\Delta=2.5$, $E=3.5$ (the rest of the parameters are the same as in Fig. 1).

These numerical results suggest that the complex dynamic behavior of Bloch walls is related with secondary instabilities of the extended roll patterns which form the domains at both sides of the wall. In particular, numerics show that bursting and spiking of the wall position always develop in coincidence with the appearance of a second spatial frequency in the intensity of the roll pattern forming one of the domains. To check this statement, Eqs. (1) and (2) were integrated in the absence of walls, and the spatial distribution of roll patterns was studied. A summary of results is given in Fig. 11, corresponding to roll patterns obtained for a fixed

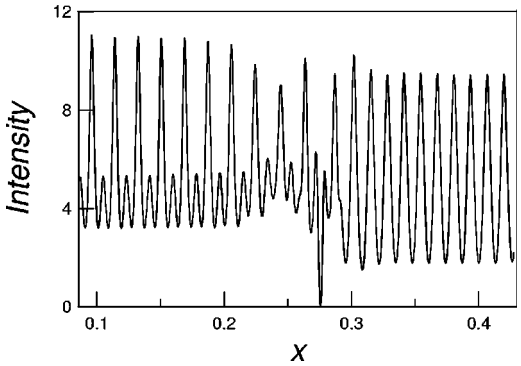

FIG. 10. Intensity distribution near a Bloch wall corresponding to Fig. 7. Note that the wall connects periodic patterns with different spatial structure.

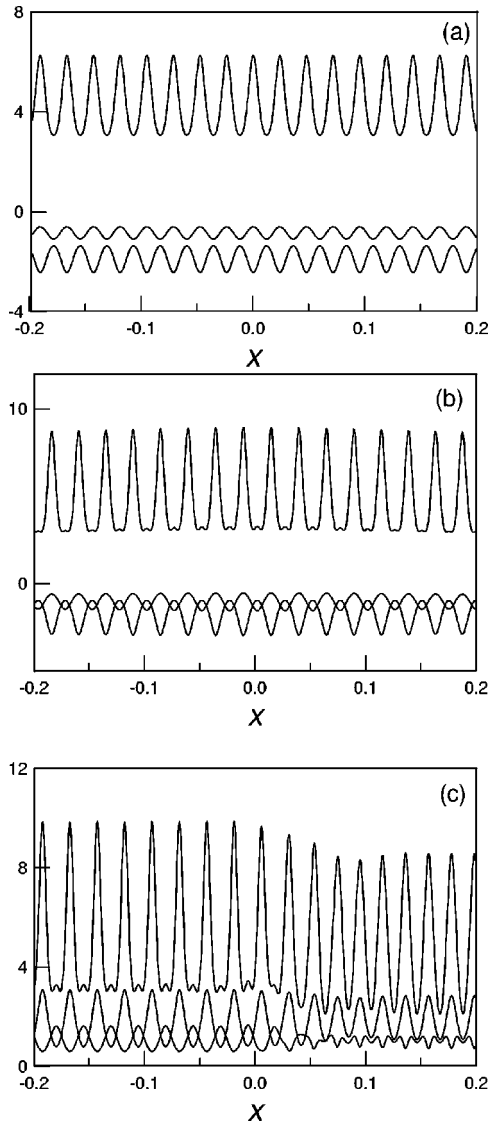

FIG. 11. Roll patterns obtained at different detunings, for $E=3.5$ (the rest of the parameters are the same as in Fig. 1). (a) Stationary roll pattern with a single spatial frequency ($\Delta=1.5$); (b) a second spatial frequency appears ($\Delta=2$); (c) bistability of roll patterns with different structure ($\Delta=2.25$). Patterns in (b) and (c) are dynamic.

value of the pump $E=3.5$ and for different detunings, in accordance with Figs. 8 and 9. The distributions shown in Figs. 11(a)–11(c) correspond, from top to bottom inside each figure, to the intensity, the real and the imaginary parts of the extended patterns. Figure 11(a) has been obtained for $\Delta=1.5$, and the resulting intensity pattern is a stationary roll, with a single spatial frequency. In Fig. 11(b), where $\Delta=2$, the intensity pattern develops a second spatial frequency of small amplitude. This value of detuning nearly corresponds to the onset of bursting phenomena of the wall. Finally, in Fig. 11(c), for $\Delta=2.25$, the resulting intensity pattern shows the coexistence, in different spatial domains, of rolls with different periodicity and equal phases (compare with Fig. 10 where a domain wall separates oppositely phased patterns). Clearly, in this parameter region there exists bistability between different spatial structures. This bistability seems to be a requirement for the existence of irregular dynamics. It is interesting to interpret these results in terms of the real and imaginary parts of the patterns shown in the bottom parts of Figs. 11(a)–11(c). The second spatial frequency of the intensity pattern, and consequently the irregular dynamical behavior, appears when real and imaginary parts of the pattern distributions cross, Fig. 11(b) and left part of Fig. 11(c).

VII. CONCLUSIONS

We have studied the dynamics of domain walls in an anisotropic optical Kerr cavity. Both Ising and Bloch walls, and the transition between them, have been reported in the case of moderate cavity anisotropy. The stability of the homogeneous solutions against pattern forming instabilities has been also analyzed. These results show a complex scenario of spatiotemporal evolution of patterns in this system. Domain wall dynamics is shown to be related with the stability of the domain (background) solutions. A numerical study shows the existence of different domains of behavior, depending on parameters. Besides the typical evolution of Bloch walls, with a drift at nearly constant velocity, we have observed regimes in which the behavior of the Bloch wall parameters (position, velocity, chirality, and intensity at the core) is irregular, and analogous to that found in the temporal dynamics of excitable systems. These regimes, namely bursting and spiking, are reported for the first time in the case of domain walls in optical cavities. Finally cavity solitons formed by the interaction of two domain walls have been identified and two dynamical regimes of wall collision have been envisaged.

ACKNOWLEDGMENTS

The authors gratefully acknowledge helpful comments by Pier Luigi Ramazza. This work was financially supported by the Spanish Ministerio de Ciencia y Tecnología and European Union FEDER, under Projects Nos. BFM2002-04369-C04-01 and BFM2002-04369-C04-04.

[1] P. Coullet, J. Lega, B. Houchmanzadeh, and J. Lajzerowicz, Phys. Rev. Lett. **65**, 1352 (1990).

[2] D. Michaelis, U. Peschel, F. Lederer, D. V. Skryabin, and W. J. Firth, Phys. Rev. E **63**, 066602 (2001).

[3] T. Frisch, S. Rica, P. Coullet, and J. M. Gilli, Phys. Rev. Lett. **72**, 1471 (1994).

[4] A. Hagberg and E. Meron, Phys. Rev. E **48**, 705 (1993).

[5] I. Pérez-Arjona, F. Silva, G. J. de Valcárcel, E. Roldán, and V. J. Sánchez-Morcillo, J. Opt. B: Quantum Semiclassical Opt. **6**, S361 (2004).

[6] G. Izús, M. San Miguel, and M. Santagiustina, Opt. Lett. **25**, 1454 (2000).
[7] Ye. Larionova, U. Peschel, A. Esteban-Martín, J. García Monreal, and C. O. Weiss, Phys. Rev. A **69**, 033803 (2004).
[8] A. Esteban-Martín, V. B. Taranenko, J. García, G. J. de Valcárcel, and E. Roldán, Phys. Rev. Lett. **94**, 223903 (2005).
[9] I. Pérez-Arjona, F. Silva, E. Roldán, and G. J. de Valcárcel, Opt. Express **12**, 2130 (2004). A. Esteban-Martín, V. B. Taranenko, J. García, G. J. de Valcárcel, and E. Roldán, Opt. Express **13**, 3631 (2005).
[10] F. T. Arecchi, S. Boccaletti, and P. L. Ramazza, Phys. Rep. **318**, 1 (1999).
[11] L. A. Lugiato and R. Lefever, Phys. Rev. Lett. **58**, 2209 (1987).
[12] J. B. Geddes, J. V. Moloney, E. M. Wright, and W. J. Firth, Opt. Commun. **111**, 623 (1994).
[13] M. Hoyuelos, P. Colet, M. San Miguel, and D. Walgraef, Phys. Rev. E **58**, 2992 (1998).
[14] R. Gallego, M. San Miguel, and R. Toral, Phys. Rev. E **61**, 2241 (2000).
[15] V. J. Sánchez-Morcillo, G. J. de Valcárcel, and E. Roldán, Opt. Commun. **173**, 381 (2000).
[16] V. J. Sánchez-Morcillo, I. Pérez-Arjona, F. Silva, G. J. de Valcárcel, and E. Roldán, Opt. Lett. **25**, 957 (2000).
[17] I. Pérez-Arjona, V. J. Sánchez-Morcillo, G. J. de Valcárcel, and E. Roldán, J. Opt. B: Quantum Semiclassical Opt. **3**, S118 (2001).
[18] G. J. de Valcárcel, I. Pérez-Arjona, and E. Roldán, Phys. Rev. Lett. **89**, 164101 (2002).
[19] S. Longhi, Phys. Scr. **56**, 611 (1997).
[20] S. Trillo, M. Haelterman, and A. Sheppard, Opt. Lett. **22**, 970 (1997).
[21] W. L. Kath, A. Mecozzi, P. Kumar, and C. G. Goedde, Opt. Lett. **19**, 2050 (1994).
[22] A. Esteban-Martín, J. García, E. Roldán, V. B. Taranenko, G. J. de Valcárcel, and C. O. Weiss, Phys. Rev. A **69**, 033816 (2004).
[23] R. W. Boyd, *Nonlinear Optics* (Academic, New York, 1992).